Scanning Electron Microscopy

Volume 3
Number 1 *3rd Pfefferkorn Conference*

Article 21

1984

The Influence of Sample and Detector Angles Upon Auger Electron Signal

Robert L. Gerlach
Perkin-Elmer

Electron Optical Systems (pp. 201-207)
SEM Inc., AMF O'Hare (Chicago), IL 60666-0507, U.S.A.

0-931288-34-7/84$1.00+.05

THE INFLUENCE OF SAMPLE AND DETECTOR ANGLES UPON AUGER ELECTRON SIGNAL

Robert L. Gerlach

Perkin-Elmer, Physical Electronics Division,
6509 Flying Cloud Drive,
Eden Prairie, Minnesota 55344, U.S.A.
Telephone Number (612) 828-6212

Abstract

The effects of the sample to incident electron beam angle and of the detector angle on the Auger electron signal are important for quantitative Auger analysis, particularly for Auger mapping and line scans. A first approximation, single scattering, mean free path model is employed to simulate the Auger signal resulting from a range of sample and detector angles. The model is single scattering in the sense that the excitation path is taken to be a straight line into the solid. A second model approximates multiple scattering by a normal distribution of ionizing flux angles about the incident beam direction.

Since spherical particles exhibit all possible surface angles, they are useful for testing the theoretical models. A coaxial electron gun/cylindrical mirror analyzer (CMA) instrument with an "angle-resolved drum" is employed to analyze 200μm diameter Ti spheres on a Sn substrate. The observations compare favorably with predictions of the model for Ti and O Auger signals, and the multiple scattering approximation is seen to more accurately describe the results.

Key Words: Auger, surface analysis, detector, microprobe

Introduction

The Scanning Auger Microprobe (SAM) has widespread acceptance in pure and applied surface science studies. The effects of surface topography and detector geometry upon the Auger signal are important in the interpretation of Auger line scans and maps. The effects of surface roughness upon Auger electron spectroscopy, where the incident beam is large compared with surface roughness dimensions, was treated by Holloway[4]. It was shown, for example, that using a coaxial electron gun in a cylindrical mirror analyzer (CMA) with electrons impinging normally upon an Au surface having grains of 21° RMS angle from the surface normal gave 10% reduced signal compared with a smooth surface. Also demonstrated was that a smooth Au surface results in less than 15% reduction in Auger signal when tilted up to 80° to the full CMA axis.

Recent SAM instruments employ microbeams of sufficiently small diameter that surface roughness (grain size) dimensions may be large compared with the probe diameter. In this case, we are sampling an individual surface geometric condition and can observe large deviations in signal. Shimizu et al [9] have used Monte Carlo methods to investigate normal and 45° incidence, 10keV electron beams on an Al surface. They predict that a 70% increase in K-ionization results in the near surface region upon tilting from normal to 45°, whereas, only a 40% increase results in the L-ionization. Only these two angles were treated by Shimizu.

In a more recent paper, Shimizu et al [10] examined, theoretically and experimentally, the effects of a sharp edge upon the Auger signal. The Monte Carlo calculation predicts an enhancement of the K and L Auger signals at the edge of an Al sample, which was also observed experimentally. This enhancement results from the fact that Auger electrons are detected from the edge which is parallel to the beam as well as from the perpendicular face.

El Gomati and Prutton [2] performed Monte Carlo calculations of normal and 75° incident

electrons upon an Al target. Figures showing trajectories of 100 electrons in the solid are shown, but no quantitative comparison for Auger signal is made for the two angles. An increase in signal for the glancing incidence is apparent from the figures, however. Both the Shimizu and Gomati papers do not account for detector geometry.

Jablonski [5] recently presented various approximations for the Auger backscattering factor as a function of sample angle utilizing Monte Carlo calculations. Results for the full cylindrical mirror analyzer detector are similar to those presented in this paper, but no analysis is given for other detector geometries. Definitive data and theoretical treatment of sample angle and detector geometry effects upon Auger signal have been lacking.

Theoretical Treatment

Single Scattering Approximation

In this section we consider the production of Auger electrons as a function of primary electron incidence angle from a smooth spherical surface. Here we consider the two detector geometries shown in Figure 1 - a full CMA about the Z-axis and a segment of the CMA towards the X-axis direction. The CMA collects electrons from 36° to 48° from the Z-axis.

Referring to Figure 2, assume in our first approximation that the incident beam travels in a straight line into the solid and that the core level excitation (production of Auger electrons) decays exponentially with path length [1,9] governed by the mean free path λ_I. Similarly we assume that the probability for Auger electron escape from the solid decays exponentially with escape length [8]. In a previous paper [3] it was shown that the following equation results for the Auger electron intensity as a function of the sample normal direction (Θ_N, ϕ_N):

$$J_{IA}(\Theta_N, \phi_N) = (J_1 \lambda_I / \lambda_e) \int_{\Omega_A} (1+\beta \cos \Theta_{IN} / \cos \Theta_{NA})^{-1} \, d\Omega_A \quad (1)$$

where λ_e is the core ionization mean free path, λ_A is the mean free path for ejected Auger electrons, $\beta = \lambda_I/\lambda_A$, Ω_A is the solid angle of ejected Auger electrons, Θ_{IN} is the angle between the incident beam and the surface normal, and Θ_{NA} is the angle between the surface normal and the ejected Auger electron.

The integration in Equation (1) is performed only over the detector solid angle. In addition, the inequalities

$$0 \leq \Theta_{IN} \leq 90^0 \quad \text{and} \quad 0 \leq \Theta_{NA} \leq 90^0 \quad (2)$$

must be satisfied.

In the typical case, β =100 such that the integrand in Equation (1) reduces to $\cos\Theta_{NA}$ $\sec\Theta_{IN}$ provided $\Theta_{IN} << 90°$. This $\cos\Theta_{NA}$ $\sec\Theta_{IN}$ relationship was discussed briefly by Janssen and Venables [6].

Approximation of Multiple Scattering

Multiple scattering and reduction of the incident flux energy are included in the Monte Carlo calculations of Shimizu et al [10] and of Gomati and Prutton [2]. If we consider Figure 1 of reference 10 and Figure 3 of reference 2, it is reasonable to assume that the incident ionizing beam I_I may be approximately described by

$$I_I = I_{IO} \, e^{-L_1/\lambda_I} \times \frac{1}{\sqrt{2\pi}\,\phi_{IO}} \, e^{-1/2(\phi_I/\phi_{IO})^2} \quad (3)$$

where L_1 is the incident beam path length into the solid. The first exponential term is as used in our first approximation (equation 1) and the second term approximates the scattering of the ionizing flux to angles ϕ_I away from the incident beam direction with a normal distribution. Hence, the equation for the Auger signal becomes

$$J_{2A}(\Theta_N, \phi_N) = (J_2 \lambda_I/\lambda_e \phi_{IO}) \int_{\Omega_A} \int_{\Omega_I} (1+\beta \cos \Theta_{IN}/\cos \Theta_{NA})^{-1} e^{-1/2(\phi_I/\phi_{IO})^2} \, d\Omega_I \, d\Omega_A \quad (4)$$

where Ω_I is the ionizing flux solid angle. Equation (4), of course, reduces to equation (1) for $\phi_{IO} = 0$.

Numerical calculations of Auger line scans across a spherical sample are shown in Figure 3, where the distance X across the sphere is normalized to unit radius. In addition, the Auger signals are normalized to the center of the sphere for each set of parameters, since we are primarily interested in the shape of the signal response. Figure 3A shows curves for the full CMA with $\beta = \lambda_I/\lambda_A$ =1000, and various ϕ_{IO} values employed in equation 4. The theory predicts relatively flat signal response over the center of the sphere and signal enhancement at the edges. The effect of increasing ϕ_{IO} is to spread the edge enhancement towards the sphere center as is obvious from the form of equation 4.

The effects of the parameter β are shown in Figure 3B for the full CMA and ϕ_{IO} = 18°. Increasing β increases the edge signal enhancement without affecting the signal function shape near the center of the sphere. As the depth of penetration of the incident beam is increased more signal is generated as the beam skims the edge of the sphere where the Auger electrons are very likely to escape and be detected.

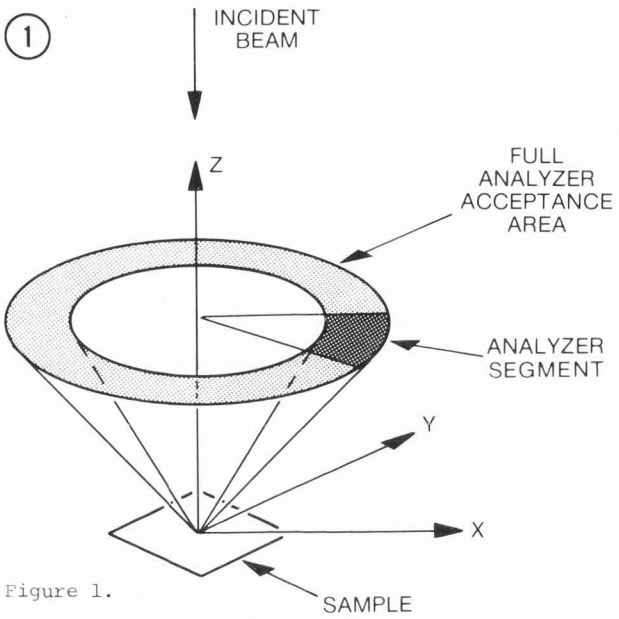

Figure 1.

Isometric drawing of the full and segmented CMA/primary electron beam geometries. In each case the Auger electrons are collected at 36° to 48° from the analyzer axis.

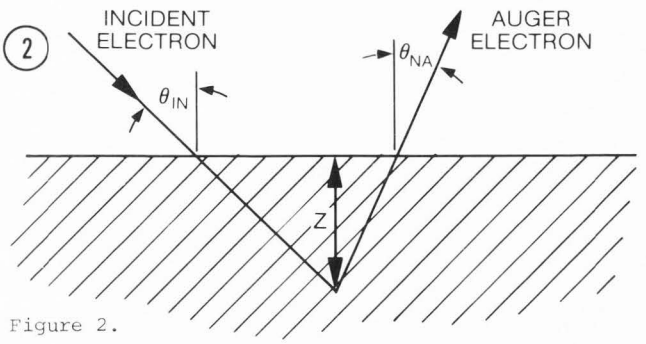

Figure 2.

Diagram of the primary electron beam and of an Auger electron escape from the solid surface.

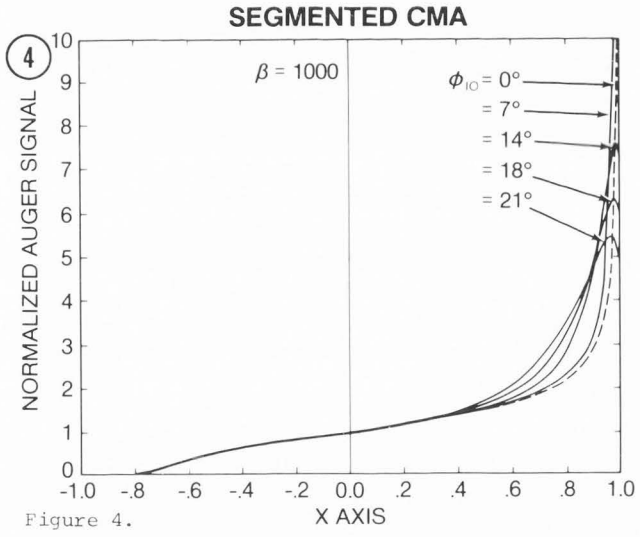

Figure 4.

Normalized Auger signal with the segmented CMA versus distance calculated from equation 4 for β = 1000 and various ϕ_{IO}.

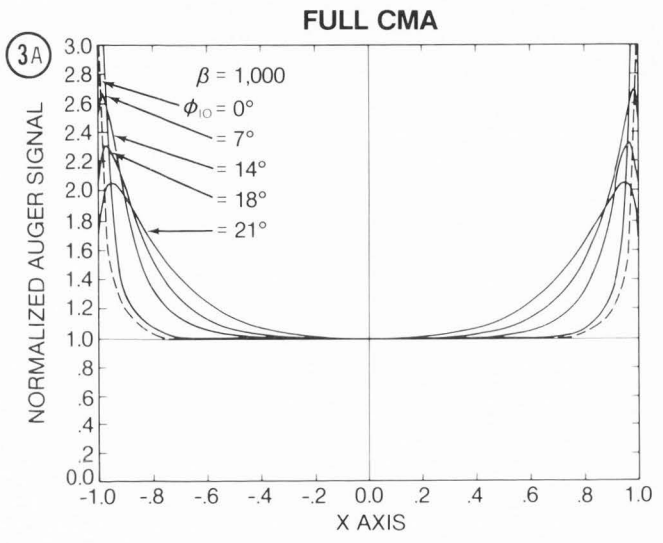

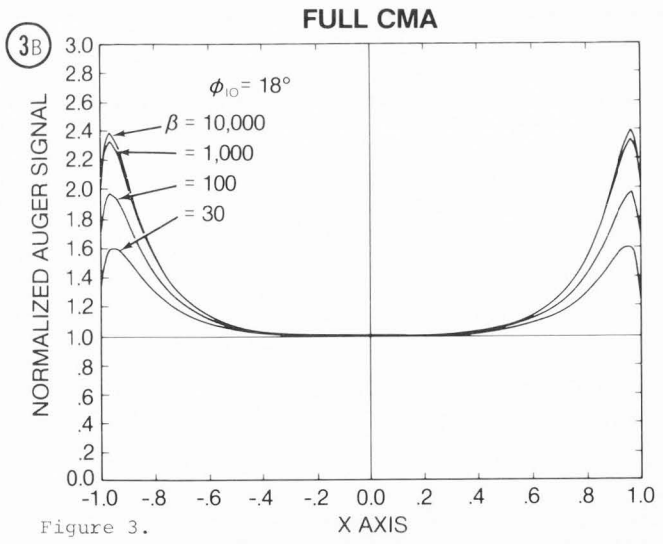

Figure 3.

Normalized Auger signal with the full CMA versus the normalized distance X across the spherical sample calculated from equation 4.

A. For β = 1000 and various incident beam half angles ϕ_{IO}.

B. For ϕ_{IO} = 18° and various β.

Calculations of the Auger signal detected by the segmented CMA (see Figure 1) are shown in Figure 4 for β = 1000 and various ϕ_{IO}. The segmented detector is blind to the left side of the sphere (shadowing effect). The signal rises rapidly with increasing X and reaches a peak near the right-hand edge of the particle. Again, increasing ϕ_{IO} spreads the edge enhancement towards the sphere center.

Comparison of Theoretical and Experimental Auger Intensities

Ti spheres of approximately 200μm diameter were dispersed onto a Sn surface and Auger analyzed with a coaxial CMA/electron gun system equipped with an "angle resolved drum". The electron gun with 4μm beam diameter at 5keV energy was scanned across the centers of the spheres and produced the Auger line scans in Figure 5, where comparisons with the theory are shown.

For comparisons of the theory with experiment we must evaluate β from the known Auger escape depth and excitation mean free path values for Ti. Since the O(KLL) and Ti(LMM) Auger electron emissions are at 503 and 418eV, respectively, their escape depths are estimated [8] to be λ_A = 10A. An estimate of the excitation mean free path from Love et al (see Figure 10 of reference 7) indicates that $\lambda_I \simeq$ 1μm for Ti at 5keV and for a 10:1 ratio for primary beam energy to ionization energy. A ratio β = 10,000 A/10A = 1000 was therefore used in our calculation. The single scattering approximation (equation 1) qualitatively describes the Auger intensities for both the segmented and full CMA. However, the rise in signal at the edges of the sphere is predicted to be too steep and too close to the edges.

Equation 4 with ϕ_{IO} = 18° and β = 1000 fits the data reasonably well as shown in Figure 5. It is physically reasonable that the scatter in the incident beam has an 18° angular divergence [2,10]. The multiple scattering approximation describes the experimental data best but still overestimates the edge enhancement. Surface roughness may account for the lack of agreement at the edges of the sphere.

Surface roughness has two effects upon the measurements. First, the surface normal $\underline{R}_N$ has a distribution about its mean value. Second, the long path lengths at grazing incidence are broken up. To simulate the second effect we limit the grazing incident angle Θ_{IN} according to the following inequality:

$$\cos \Theta_{IN} > 0.03.$$

Physically this limits the grazing incidence to approximately $33\lambda_A \simeq$ 330 Å. The resulting curves shown in Figure 5 fit the experimental data reasonably well.

A two dimensional Ti Auger map of the Ti sphere is shown in Figure 6 where the segmented detector was employed. Also shown is a contour map calculated from equation 4 which shows good correspondence to the experimental map.

Other Applications of the Model

Now that we have established that this empirical model describes the Ti sphere data, it is interesting to apply it to other geometries. It should be emphasized that though we have not proven equation 4 to be valid for a range of materials, surface smoothness, and a wide range of ϕ_N, it should give us a qualitative representation. As a first case we examine the effect of placing a segmented (or point) detector at various angles ϕ_D with respect to the primary electron beam axis. Results of this calculation are shown in Figure 7, where the abscissa is now the polar angle ϕ_N of the surface normal (instead of the distance across a sphere). One sees that if the detector could be placed very near the primary beam axis (ϕ_D = 0), then the Auger signal would be relatively insensitive to the sample angle except that the signal falls to zero for ϕ_N = ±90°. As the detector angle ϕ_D is increased, the signal versus sample angle curve becomes increasingly asymmetric and peaked towards the detector side. The signal is cut off for ϕ_N <($-90° + \phi_D$).

Consider next the effect of the sample holder plane being tilted angle ϕ_S as shown in Figure 8. When the full CMA detector is used, the left-hand side of the detector begins to be cut off to input signal when $\phi_S \simeq \phi_{CMA}$ = 42°. The effects of this are shown in Figure 9 where for computational convenience the CMA is modelled as having entrance angle ϕ_{CMA} =42° with very small Δφ. One sees that for ϕ_S < 42° the signal is an asymmetric function of ϕ_N. When ϕ_S = 60°, the signal for ϕ_N = -60° is less than half that for ϕ_N = +60°.

Typical surfaces are not like Figure 8, where a single sphere lies upon a flat surface at angle ϕ_S, but rather many hills and valleys populate the surface. As a result a hill may tend to shadow another surface feature to angle ϕ_S, producing a loss of signal as represented in Figure 9.

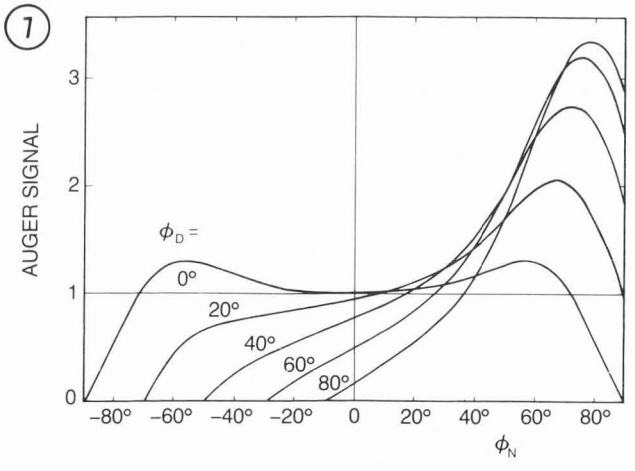

Figure 7.
Computed Auger signal as a function of the sample normal polar angle ϕ_N for various detector polar angles ϕ_D, where ϕ_N, ϕ_D and the Z axis are in the same plane. The curve for ϕ_D = 0 is arbitrarily normalized to unit signal at ϕ_N = 0.

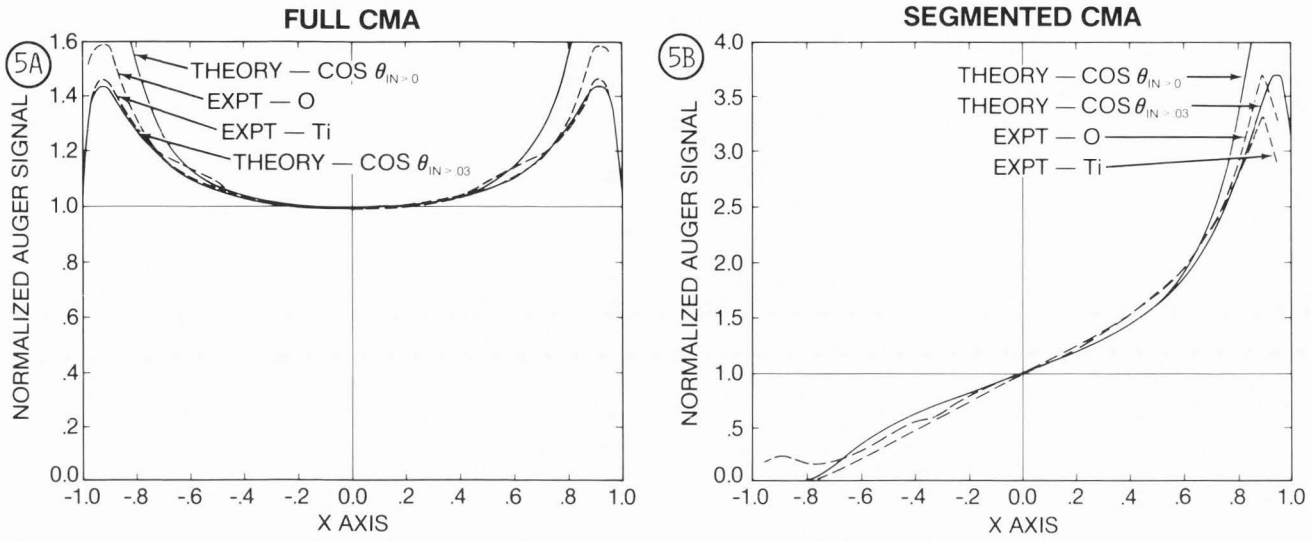

Figure 5. Comparison of theoretical and experimental Auger signal for a line scan across a Ti sphere. The theoretical curves were computed from equation 4 with β = 1000 and ϕ_{IO} = 18°.

A. Full CMA.

B. Segmented CMA.

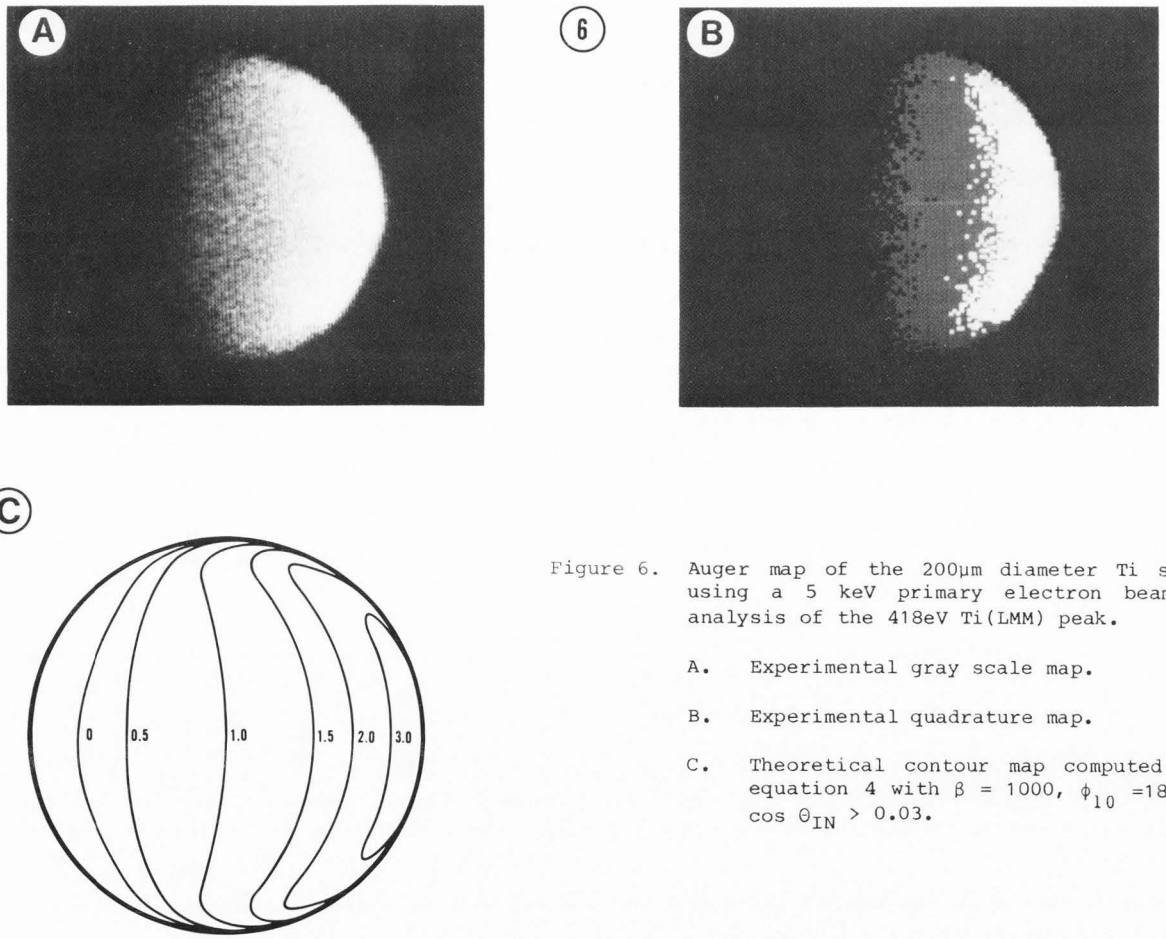

Figure 6. Auger map of the 200μm diameter Ti sphere using a 5 keV primary electron beam and analysis of the 418eV Ti(LMM) peak.

A. Experimental gray scale map.

B. Experimental quadrature map.

C. Theoretical contour map computed from equation 4 with β = 1000, ϕ_{10} =18° and cos Θ_{IN} > 0.03.

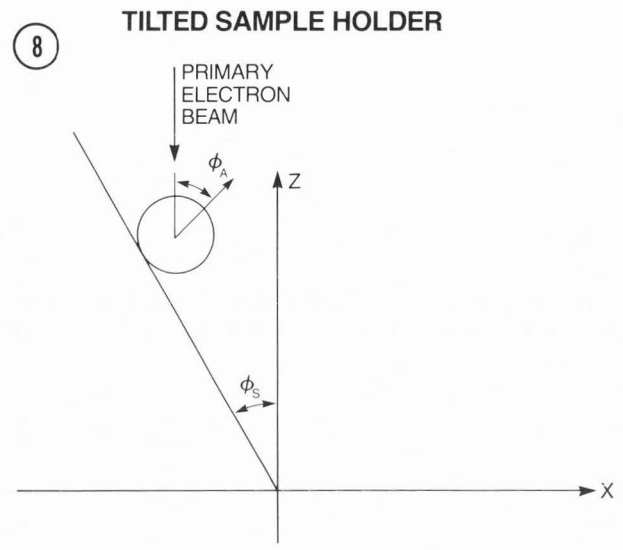

Figure 8.

Diagram of a small sphere on a sample holder tilted at polar angle ϕ_S.

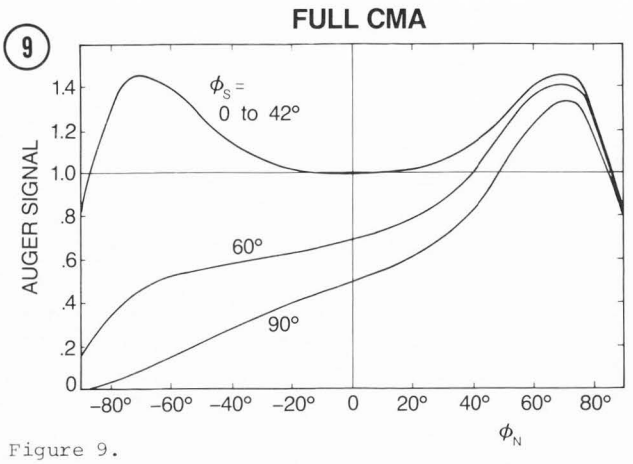

Figure 9.

Computed Auger signal as a function of the sample normal polar angle ϕ_N for various sample holder tilt angles ϕ_S, where ϕ_N, ϕ_S and the Z axis are in the same plane. The curve for ϕ_S = 0 to 42° is arbitrarily normalized to unit signal at ϕ_N = 0.

Conclusions

As a small solid angle detector is brought closer to the primary beam axis, the Auger signal versus sample angle (ϕ_N) curve becomes increasingly symmetric, though the signal at ϕ_N = ±90° goes to zero. However, the detector axis must be within about 20° of the gun axis to give reasonably flat response, which is not a very feasible angle experimentally.

In using the full CMA detector, surface topography and large sample holder tilt angles can block the signal to the CMA. However, there is no signal reduction until an adjacent surface feature is within the $\phi_{CMA} \simeq 42°$ cone angle of the detector.

Finally, various means are in use to correct for this loss of signal due to surface topography. The most common methods employ the normalization of the Auger signal by the background energy distribution. These methods can be successful provided there is of course a signal from the region of interest and that the corrections are relatively small (≃2x).

References

1. Dudek HJ (1980). Influence of the Electron Beam Angle of Incidence on the Spatial Distribution of the Ionization Density. Proceedings of the Seventh European Congress on Electron Microscopy, The Hague, Netherlands, Aug. 24-29, 1980. Editors P. Brederoo and V.E. Cosslett. Volume 3, 7th European Congress on EM Foundation, Leiden, 22-23.

2. El Gomati MM. and Prutton M. (1978). Monte Carlo Calculations of the Spatial Resolution in a Scanning Auger Electron Microscope. Surface Sci. 72, 485-494.

3. Gerlach RL, Hovland CT, Clough SP, Pinchback TR. (1982). Scanning Auger Electron Images with Orthogonal Versus Coaxial Gun/Analyzer Geometry. 10th International Congress on Electron Microscopy, Hamburg, (ed.) The Congress Organizing Committee, Volume I, Deutsche Gesellschaft fur Electronenmikroskopie, Frankfurt. 719-720.

4. Holloway PH. (1975). The Effect of Surface Roughness on Auger Electron Spectroscopy. J. Electron Spectroscopy and Related Phenomena 7, 215-232.

5. Jablonski A. (1983). Dependence of the Backscattering Factor in AES on the Primary Electron Incidence Angle. Surface Sci. 124, 39-50.

6. Janssen AP, Venables JA. (1978). The Effect of Backscattered Electrons on the Resolution of Scanning Auger Microscopy. Surface Sci. 77, 351-364.

7. Love G, Cox MGC, Scott VD. (1977). A Simple Monte Carlo Method for Simulating Electron-Solid Interactions. J. Phys. D: Appl. Phys. 10, 7-23.

8. Palmberg PW. (1973). Quantitative Analysis of Solid Surfaces by Auger Electron Spectroscopy. Analytical Chemistry 45, 549A-556A.

9. Shimizu R, Aratama M, Ichimura S, Yamazaki Y. (1977). Application of Monte Carlo Calculation to Fundamentals of Scanning Auger Electron Microscopy. Appl. Phys. Lett. 31, 692-694.

10. Shimizu R, Everhart TE, MacDonald NC, Hovland CT. (1978). Edge Effect in High-Resolution Scanning Auger-Electron Microscopy. Appl. Phys. Lett. 33, 549-551.

Discussion with Reviewers

M.P. Seah:
In many practical instances we may take β to be very large. Thus, for instance Figure 3(a) may be taken to represent the practical result expected for various $\Phi_{10}.\Phi_{10}$ should be a unique value for a given primary electron beam energy, atomic weight and core level ionization energy. It would be interesting in such a three dimensional space, to visualise the contours of surfaces of constant Φ_{10}. Would the author like to comment on the shapes of these surfaces so that the reader can extend the theory presented to other materials, beam energies and transitions?

Author:
Such three dimensional surfaces could be quite valuable. However, without a detailed study of these parameters, it would be premature for me to comment on the surface shape.